RSC Advances

ROYAL SOCIETY OF CHEMISTRY

www.rsc.org/advances

Journal Name

ARTICLE

Fabrication and Modeling of an Ultrasensitive Label Free Impedimetric Immunosensor for Aflatoxin B_1 based on Poly(o-phenylenediamine) Modified Gold 3D Nano Electrode Ensembles

Received 00th January 20xx,
Accepted 00th January 20xx

DOI: 10.1039/x0xx00000x

www.rsc.org/

Haifeng Hu,[a] Lixin Cao,*[a] Qingchuan Li,[a] Kan Ma,[a] Peisheng Yan[b] and Donald W. Kirk[c]

An ultrasensitive label free impedimetric immunosensor for AFB_1 detection was fabricated based on Poly(o-phenylenediamine) (PoPD) electropolymerized film modified gold three dimensional nanoelectrode ensembles (3DNEEs). The nanoelectrode ensembles were fabricated by template synthesis in track etched polycarbonate (PC) membranes. Scanning electron microscopy and X-ray diffraction were used for the evaluation of the properties of 3DNEEs. Anti-AFB_1 was directionally immobilized on Staphylococcus protein A (SpA) with orientation function. Cyclic voltammetry and electrochemical impedance spectroscopy were employed to characterize the fabrication process and optimize working conditions. The interface model of molecular recognition was constructed and reasonably interpreted. The detection limit was 0.019 ng/mL (S/N=3). The linear detection concentration range of AFB_1 was from 0.04 to 8.0 ng/mL.

1.Introduction

Aflatoxins (AFs) are a group of chemically related mycotoxins produced by Aspergillus flavus and A. parasiticus.[1] AFB_1, AFB_2, AFG_1, and AFG_2 have been classified as number one carcinogens by the International Agency for Research on Cancer (IARC). Among these, AFB_1 is the most potent carcinogenic, mutagenic, teratogenic, and immunosuppressive agent.[2-4] As a result, most countries have set strict maximum tolerable levels for foods and animal feeds. The European Union established that 2 ng/g of AFB_1 alone is the maximum amount permitted. One of the most effective methods to avoid the hazard of AFB_1 is to develop fast and accurate detecting technology.[5] The common established methods for AFB_1 detection, such as high performance liquid chromatography,[6] radioimmunoassay or enzyme-linked immune sorbent assay[7, 8] are relatively complex, time-consuming, and need skilled operators, expensive equipment or radioactive materials. Therefore, studies have been concentrated on establishing methods which are simpler, quicker and have higher sensitivity with lower cost.

In recent years, researchers have focus on the design and construction of electrochemical biosensors for AFB_1 detection, such as immunosensors,[9] enzyme biosensors[10] and DNA biosensors.[11, 12] Among them, the electrochemical immunosensor has attracted much interest for its high sensitivity and selectivity because it combines the advantages of electro analysis and immunoreaction which are based on specific recognition and combination. Compared with other sensors, the impedimetric immunosensor is more direct, time saving and simple. Moreover, it is also characterized by being label-free, requiring no special reagents, being time saving, and working at lower voltages.[13-15] However, further research work should be done to improve the selectivity and stability.

The electrode is the core of an electrochemical biosensor, at which the antibody or antigen is immobilized, and the antigen-antibody combined reaction signal is converted to an electrochemical signal. Its structure, surface condition and electrochemical properties are the crucial factors for the performance of the electrochemical biosensor[16]. In recent years, three dimensional structured nanoelectrode ensembles (3DNEEs) have attracted considerable interest[17] for their outstanding performances in biosensors[18, 19] and electrocatalysis[20-22] mainly due to their special configurations and large surface areas.[23-25]

The construction of a biomolecule recognition membrane, on which antibody and antigen are effectively immobilized and recognized, is crucial step for a biosensor assembly. One efficient method is to functionalize the electrode to immobilize as much recognition molecule as possible. Literatures and our previous work showed that PoPD (Poly(o-phenylenediamine)) modified electrodes have good performance in immunosensor,[26, 27] because it is conductive, ultrathin, self-limiting and has more amino and imino groups, which is beneficial in binding more antibody. Another direction is to make the binding site of the recognition molecules exposed to

[a] Department of Applied Chemistry, Harbin Institute of Technology, Weihai campus, Wenhuaxi Road, Weihai, Shandong, 264209 China
[b] Department of Bioengineering, Harbin Institute of Technology, Weihai campus, Wenhuaxi Road, Weihai, Shandong, 264209 China
[c] Department of Chemical Engineering and Applied Chemistry, University of Toronto, 200 College Street, Toronto, Ontario, M5S 3E5 Canada
E-mail: caolixin668@aliyun.com; Tel: +86 631 5687232; Fax: +86 631 5687232

be oriented in order to construct an immunosensor with high specificity, sensitivity, and stability. Employing Staphylococcal protein A (SpA) was considered to be an efficient method.[28-30] The purpose of this paper is to fabricate a label-free AFB_1 impedimetric immunosensor using PoPD modified 3DNEEs (PoPD/3DNEEs), taking the combined advantages of the special structure and large active surface area of 3DNEEs, and functionalizing features of the PoPD. The effective biomolecule recognition membrane was constructed with the help of Staphylococcal protein A to expose the binding site of anti-AFB_1 directionally for combining AFB_1 efficiently. The work on the AFB_1 immunosensor will not only determine its potential for AFB_1 detection but also for its application in immunosensors.

2. Experimental

2.1 Reagents and equipment

Aflatoxin B_1, Aflatoxin B_1 antibody (from rabbit) and Staphylococcus protein A were purchased from Sigma-Aldrich Co (USA). Glutaraldehyde (GA, 50% solution in water) and Bovine serum albumin (BSA) were obtained from Sangon Biotech Co (China). *O*-phenylenediamine (*o*PD) was from Sinopharm Chemical Reagent Co (China). The gold plating solution used as a standard plating solution known as Oromerse Part B containing sodium gold sulphite ($Na_3Au(SO_3)_2$), was obtained from Technic Inc. A mixture of methanol and ultrapure water (V/V=2:8) was used as AFB_1 diluent. All chemicals used were of analytical grade and were used as received without any further treatment. For solution, ultrapure water with a specific resistance over 18 $M\Omega \cdot cm^{-1}$ was used throughout the study.

SPI polycarbonate (PC) membranes with a density of ca. (1-5) $\times 10^8$ pores/cm^2 and 100 nm in diameter from Nucleopore track-etching were obtained from Whatman. SEM and EDX images were obtained using scanning electron microscopy (Hitachi S-4700, Japan). The XRD experiment was recorded using an x-ray diffractometer (DX-2700, China). All electroanalytical measurements were performed with a CHI 660E (Shanghai, China) at room temperature using a three-electrode single-compartment cell equipped with a platinum counter electrode and Hg/Hg_2SO_4 (K_2SO_4 saturated) (SSE) reference electrode.

2.2 Fabrication of P*o*PD/3DNEEs

Fabrication of 3DNEEs. The fabrication of 3DNEEs followed the procedure as in our previous paper[24] and literature.[25, 31] However due to the high activity of the newly made Oromerse Part B gold plating solution, an updated electroless deposition was used for gold growth in the nano pores of PC membranes. An optimized gold plating solution was prepared by dissolving Na_2SO_3 (0.13 mol/L), 1.5 mL formaldehyde (0.42 mol/L) and 1 mL of Oromerse Part B gold solution in 40 mL water. The pH value of this solution was adjusted to 11.00±0.50. The deposition procedure was carried out by immersing the PC membrane pre-prepared to the gold plating solution and kept at 4 ℃ for 24 hours.

After deposition, the membrane was purified by immersed in 25% HNO_3 for 12h. The 3DNEEs was constructed and reported as in our previous work.[23] The 3DNEEs prepared was 100 nm in diameter and 300 nm in height, its geometric area exposed to the electrolyte was 0.07 cm^2 and the theoretical calculated area was 0.0187 cm^2. Its real active area considering the micro-roughness was 0.756 cm^2, which was evaluated from the electrical redox quantity of 3DNEEs in 0.5 mol/L H_2SO_4. The detailed calculation has been given in our previous work.[24]

Development of PoPD/3DNEEs. Prior to modification, the 3DNEEs was cleaned by voltammetrically cycling, between -0.20 and +1.2 V vs. SSE at a scan rate of 50 mV/s in 0.5 mol/L H_2SO_4 until a stable cyclic votammogram was obtained.

Electropolymerization of P*o*PD was performed by voltammetrically cycling as our previous work.[26] The optimized parameters were as follows: the sweep potential range was between -0.60 to 1.0 V vs. SSE with a scan rate of 50 mV/s, in 40 mL 0.1 mol/L H_2SO_4 containing 10 mmol/L *o*-phenylenediamine. The electrosythesis was finished after 30 cycles.

2.3 Assembling of AFB_1 immunosensor

The construction procedure and optimized parameters for immunosensor BSA/anti-AFB_1/GA/P*o*PD/3DNEEs were as follows: the P*o*PD/3DNEEs as-prepared was cross-linked with glutaraldehyde by immersing the P*o*PD/3DNEEs in 5.0 mL 2.5% glutaraldehyde. Then 50 μL of 0.10 mg/mL SpA solution was dropped onto the glutaraldehyde activated electrode surface and incubated for 1 h. The immobilization of anti-AFB_1 was accomplished by adding 30 μL 1.2 mg/mL anti-AFB_1 solution to the electrode surface and incubating for another 1 h. The non-specific binding sites and deactivation of GA on the GA/ P*o*PD modified 3DNEEs were blocked using BSA (forming BSA/anti-AFB_1/GA/ P*o*PD/3DNEEs) by immersing the electrode in 5.0 mL 3% BSA solution for 40min. The electrode was washed with PBS between each step.

2.4 Detection of AFB_1

The optimized AFB1 detection processes and parameters for immunoreaction, EIS measurement and biosensor regeneration were optimized as follows. The immunosensor was incubated in AFB_1 diluents with various concentrations in a water bath at 25℃ for 40 min, washed with PBS, and then put into 0.05 mol/L Na_2SO_4 + 0.2 mol/L NaH_2PO_4-Na_2HPO_4 (PBS, pH 7.00) solution. EIS was carried out at DC potential of -150 mV vs. open circuit potential (OCP), an amplitude of 5 mv, and frequencies ranging from 100 kHz to 0.01 Hz. The immunosensor was regenerated after each detection by immersing in a 0.20 mol/L glycine-HCl buffer (pH 2.60) for 15 min. It is emphasized that rubber gloves are needed throughout the experiment and any containers contacted with AFB_1 should be disinfected in a solution of sodium hydroxide (0.5 g/mL) and sodium hypochlorite (mass ratio of 4%) after the experiment.

3. Results and discussion

3.1 3DNEEs characterizations

The morphology, structure and composition of 3DNEEs prepared are shown in Fig. 1. The SEM image of the continuous uniform gold nanowires with microroughness is shown in Fig. 1 (A) and the structure and morphology of 3DNEEs after partial chemical etching is shown in Fig. 1 (B). The Au nanowires protruding from the PC template had good parallel orientation and regular arrangement.

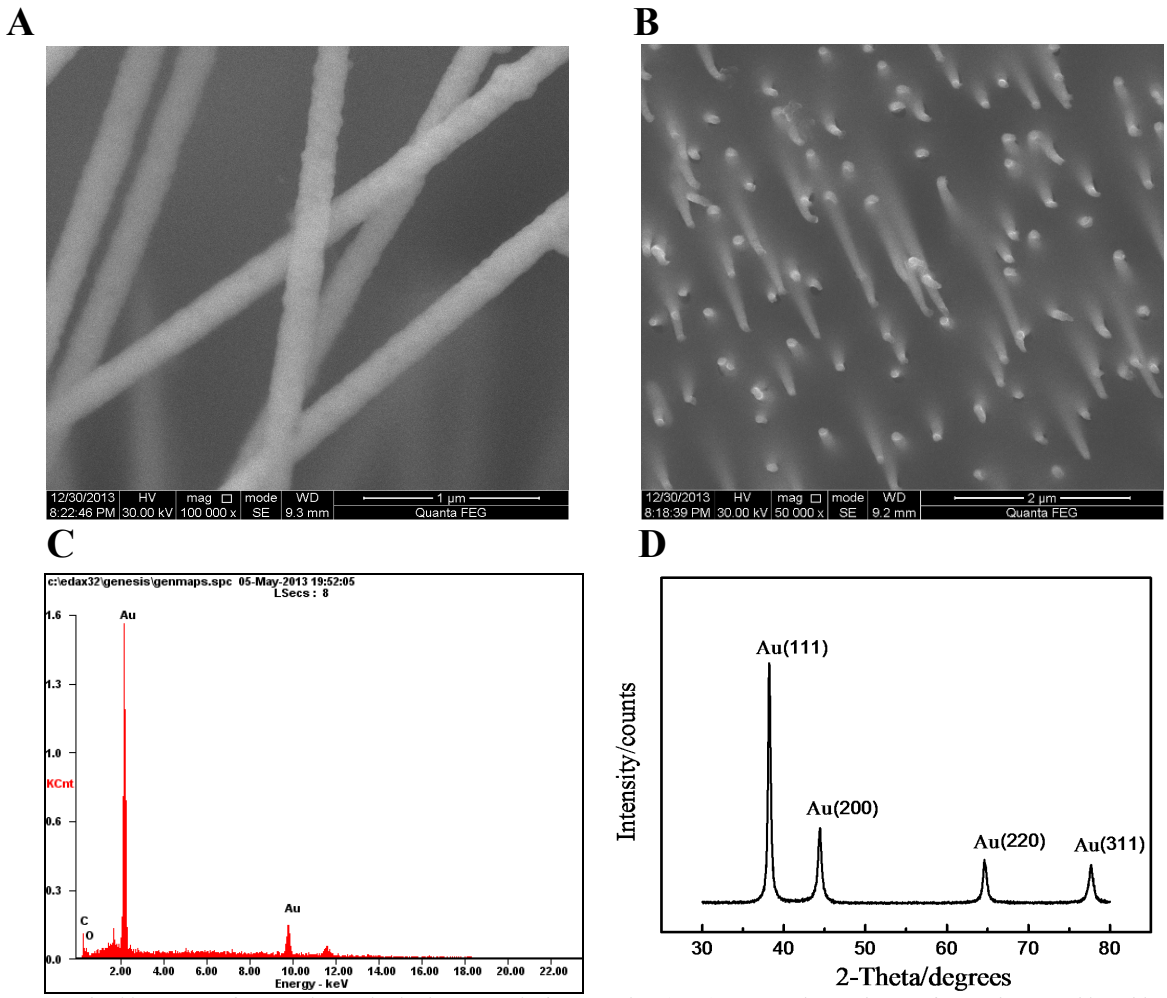

Fig. 1. SEM of gold 3DNEEs after complete and selective removal of PC template (A, B); EDX and XRD image of nanowire ensembles with 100 nm in diameter (C, D).

As shown in the EDX image of NEEs (Fig. 1 (C)), there is only a gold signal and no evidence of Sn or Ag impurities. The peak C and O were caused by the residual of PC template after complete removal. The results indicate that the 3DNEEs prepared in our work have a high purity. The XRD analysis of the deposited membrane after removing the surface layer of gold from the membrane is given in Fig. 1 (D). Only x-ray diffraction peaks of gold is found in the XRD image. The gold lattice constant calculated by software Jade is 4.078 Å, very closed to the standard gold lattice constant 4.079 Å.

3.2 Development of P*o*PD modified 3DNEEs

The cyclic voltammetry (CV) was employed for *o*PD electropolymerization on 3DNEEs and macro gold disk electrode (MGE) with geometric area of 0.07 cm^2. The results are shown in Fig. 2. In the positive potential region, peak 1 and 2 identified are related to *o*PD oxidation,[32] peak 3 and 4 are related to redox process of gold. In the negative potential region, peak 5 and 6 are related to an electron transfer process coupled with proton exchange between the P*o*PD film and the solution, possibly involving internal structural changes of the P*o*PD film.[33]

The peak current density on 3DNEEs in each position is significantly greater than that on MGE. Due to the inhibition of the P*o*PD produced in the first cycle, Peak 1 and 2 on MGE rapidly decreased in the subsequent potential cycles (the ratio of the peak current of the second cycle to the first cycle is 29.36%), while the peak on 3DNEEs reduced less (the ratio is 47.79%). This could be ascribed to the micro roughness of 3DNEEs surface, the large active area and high activity.[17] Thus, P*o*PD electropolymerization on 3DNEEs had the advantage of making full use of the micro-areas. As a result, the P*o*PD on 3DNEEs is more stable and has more active groups.

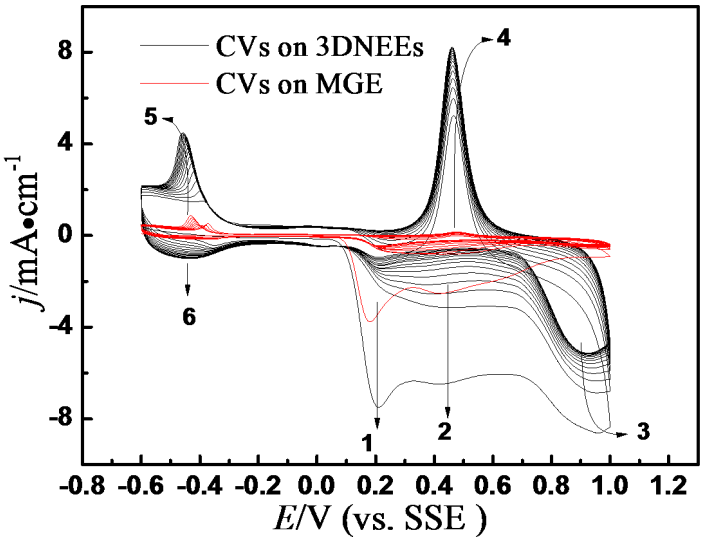

Fig. 2. Cyclic voltammograms of the electropolymerization of oPD on MGE and 3DNEEs in 10 mmol/L oPD + 1.0 mol/L H2SO4 at a scan rate of 50 mV/s. Peak 1 to 6 are described in the text.

The peak current density on 3DNEEs in each position is significantly greater than that on MGE. Peak 1 and 2 on MGE rapidly decreased in the subsequent potential cycles (the ratio of the peak current of the second cycle to the first cycle is 29.36%), while the peak on 3DNEEs reduced less (the ratio is 47.79%). This could be ascribed to the micro roughness of 3DNEEs surface, the large active area and high activity.[17] Thus, P*o*PD electropolymerization on 3DNEEs had the advantage of making full use of the micro-areas. As a result, the P*o*PD prepared on 3DNEEs is more stable and has more active groups.

The cycle of CV for *o*PD electropolymerization on 3DNEEs was optimized by the OCP of P*o*PD/3DNEEs. Table 1 shows the OCP vs. SSE with different electropolymerizing cycles in 40 mL 0.1 mol/L H_2SO_4 containing 10 mmol/L *o*-phenylenediamine. The OCP of P*o*PD/3DNEEs shifts anodically with the increasing of electropolymerizing cycles and stabilizes at around -0.12 V after 30 cycles. So 30 cycles was selected for the development of P*o*PD/3DNEEs.

Table 1 OCP of PoPD/3DNEEs with different electropolymerizing cycles in 0.1 mol/L H2SO4

Cycles	10	15	20	25	30	35	40	45
OCP/V	-0.160	-0.145	-0.132	-0.125	-0.121	-0.123	-0.119	-0.122

3.3 Fabrication of immunosensor

The AFB_1 immunosensor based on P*o*PD/3DNEEs was constructed using several steps including cross linking, incubation, immobilization, blocking and immunity reaction. The detailed assembly process and immunity of the AFB_1 immunosensor based on 3DNEEs is summarized in Fig. 3. Step (a) shows the electropolymerization of P*o*PD on 3DNEEs forming P*o*PD/3DNEEs. Step (b) shows nucleophilic addition reactions between aldehyde groups of Glutaraldehyde (GA) and aromatic amine groups of P*o*PD by Schiff bases,[34] forming GA/ P*o*PD/3DNEEs. The SpA was also immobilized to the electrode by Schiff base formation between the other aldehyde groups of GA and amine groups of SpA in step (c), forming SpA/ GA/ P*o*PD/3DNEEs. Then anti-AFB_1 is orientationally immobilized by specially binding the crystalline fragment (Fc fragment) with SpA in step (d), forming anti-AFB_1/SpA/ GA/ P*o*PD/3DNEEs. BSA plays the role of blocking nonspecific adsorptions in step (e), forming BSA/anti-AFB_1/SpA/GA/P*o*PD/3DNEEs. The formation of bioaffinity complex between antigen AFB_1 and antibody anti-AFB_1 is shown in step (f), forming AFB_1/anti-AFB_1/SpA/GA/P*o*PD/3DNEEs. Due to the three-dimensional structure and large active area of 3DNEEs, many more biomolecules were incubated on the electrode. In addition, SpA has five binding sites which can be strongly combined with Fc fragments of an antibody independently.[30, 35] Consequently, the binding sites of the combined antibody (anti-AFB_1) tend to be identical with that of the antigen AFB_1, which is crucial for improving the specificity and combining ability of bio-recognition membrane of immunosensor with high sensitivity.

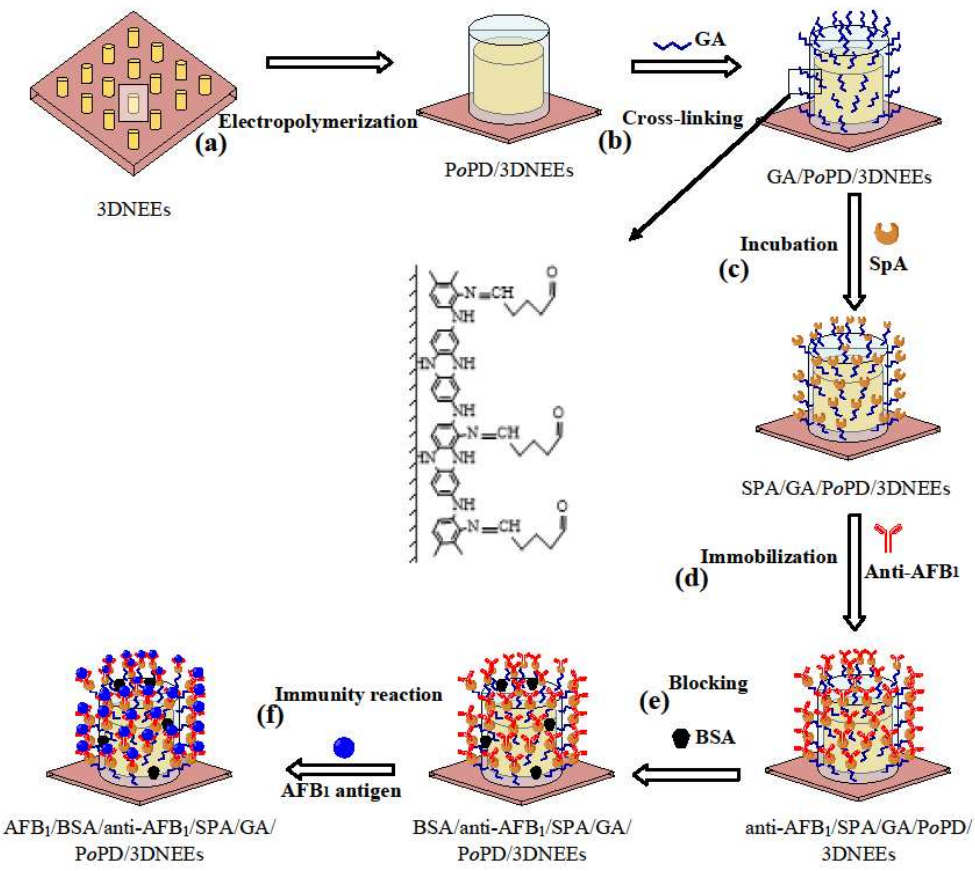

Fig. 3. Schematic diagram of the immunosensor fabrication procedures and immunity of the AFB_1 immunosensor based on 3DNEEs.

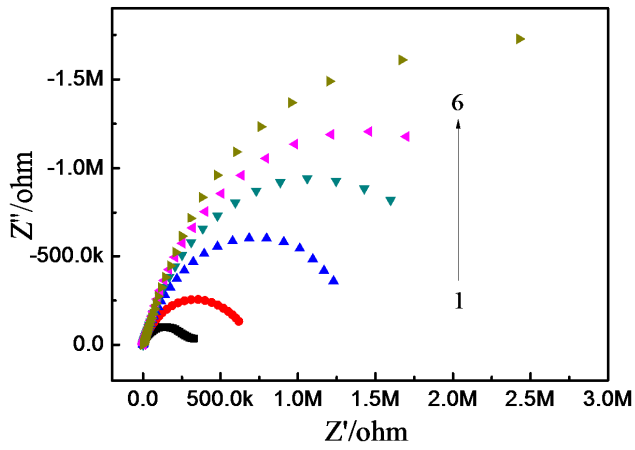

Fig. 4. Nyquist plots of immunosensor assembling at different stage in PBS (pH 7.00) with the frequency ranging from 10 mHz to 100KHz at -450 mV vs. SSE, (1) PoPD/3DNEEs, (2) GA/PoPD/3DNEEs, (3) SpA/GA/PoPD/3DNEEs, (4) anti-AFB_1/SpA/GA/PoPD/3DNEEs, (5) BSA/anti-AFB_1/SpA/GA/PoPD/3DNEEs, (6) AFB_1/BSA/anti-AFB_1/SpA/GA/PoPD/3DNEEs.

The electrodes in each step of the fabrication of immunosensor were characterized by EIS. As shown in Fig. 4, the interfacial charge transfer resistance increased continually at PoPD/3DNEEs, GA/PoPD/3DNEEs, SpA/GA/PoPD/3DNEEs, anti-AFB_1/SpA/GA/PoPD/3DNEEs, BSA/anti-AFB_1/SpA/GA/PoPD/3DNEEs, AFB_1/BSA/anti-AFB_1/SpA/GA/PoPD/3DNEEs. This could be ascribed to the blocking layer coating on electrode surface, growing thicker and thicker with the assembly procedure. The access of H^+ was hindered and the charge transfer resistance increased accordingly, indicating that the immunosensor has been successfully assembled.

To fabricate a well-performed immunosensor, the SpA incubation time and the anti-AFB_1 immobilization time were investigated in our work. As shown in Fig. 5 (A), the interfacial charge transfer resistance increased with the growth of incubation time and became almost stable after 60 min, indicating the amount of SpA immobilized on GA/PoPD/3DNEEs increased within 60 min and saturated after 60 min. As a result, the SpA incubation time used for the work was 60 min.

Nyquist plots of anti-AFB_1 immobilization on SpA/GA/PoPD/3DNEEs are shown in Fig. 5 (B). The

interfacial charge transfer resistance increased slightly after 40 min, and became almost constant after 60 min. The optimal immobilization time of anti-AFB_1 was chosen as 60 min.

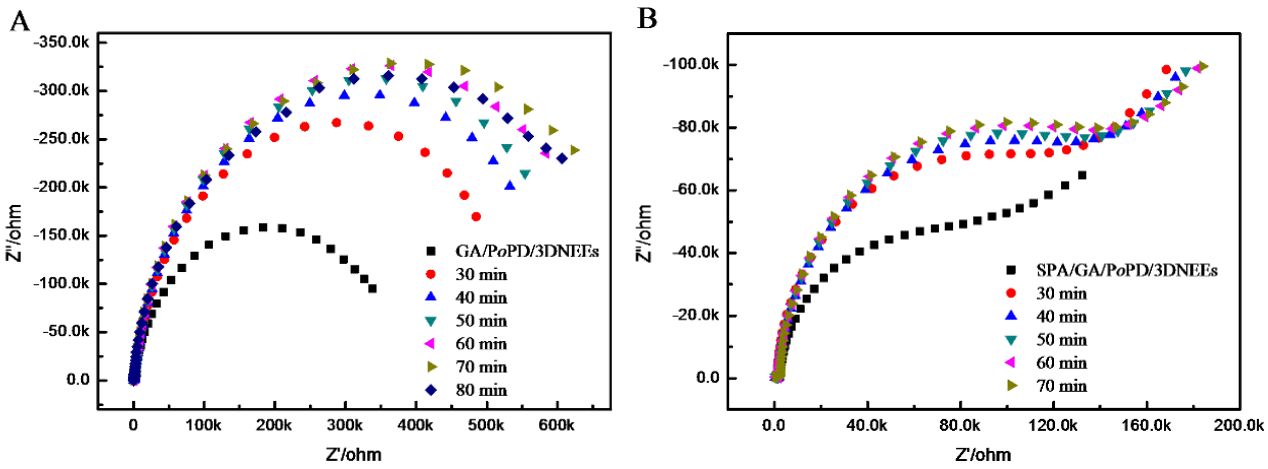

Fig. 5. Nyquist plots of GA/PoPD/3DNEEs at different SpA incubating times in 0.2 mol/L PBS (pH 7.00) (A) and Nyquist plots of SpA/GA/PoPD/3DNEEs at different anti-AFB_1 immobilizing times in 0.2 mol/L PBS (pH 7.00) (B), at -450 mV vs. SSE with the frequency range from 10 mHz to 100KHz.

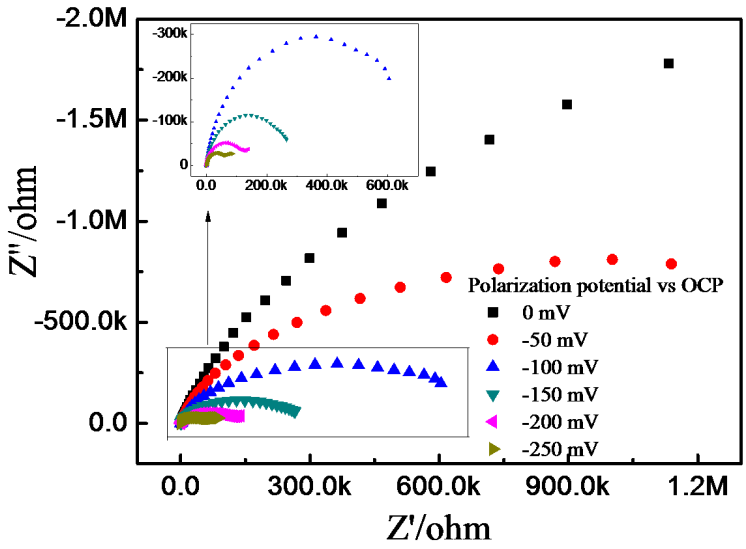

Fig. 6. Nyquist plots of the immunosensor with varying polarization potentials in 0.2 mol/L PBS (pH 7.00) at the frequency range from 10 mHz to 100 KHz, OCP: -350 mV vs. SSE.

Before initiating the biosensing test, it was important to determine how different polarization potentials might influence specific immunity response due to the charged protein molecules of the biosensor. Thus polarization potentials ranging from 0 to -250 mV vs. OCP for EIS measurement were investigated for AFB_1 detection. As shown in Fig. 6, the interfacial charge transfer resistance decreases with the potential shifting cathodically due to the good-conductivity of PoPD in negative potential range.[36] The semi-circle could be identified only when the potential was below -50 mV. Taking the immunosensor sensitivity and the integrity of the Nyquist plot into consideration, the optimized polarization potential for AFB_1 detection was chosen to be -150 mV vs. OCP. Additionally, as shown in Fig. 2, the peak current of PoPD redox related to the extraction and insertion of proton appeared at this potential.

3.4 Modeling of the immunosensor and detection of AFB_1

The software Zsimpwin was employed for simulation of EIS results. The equivalent circuit is shown in Fig. 7 (A). The Nyquist plots and Bode plots of the immunosensor in PBS (pH 7.00) after immunity with 1 μg/mL AFB_1 solution and its simulation results are shown in Fig. 7 (B, C) and fitted well in all frequency ranges. There were three elements in series in the equivalent circuit, consisting of 3DNEEs\PoPD, biorecognition film (GA\SpA\anti-AFB_1) and solution resistance from the left

to right, respectively. R_{film} and Q_{film}[37] represented film resistance and capacitance of P*o*PD; R_{brf}, Q_{brf} and W charge transfer resistance and capacitance of biorecognition film and its Warburg resistance; R_{SOL} represents solution resistance.

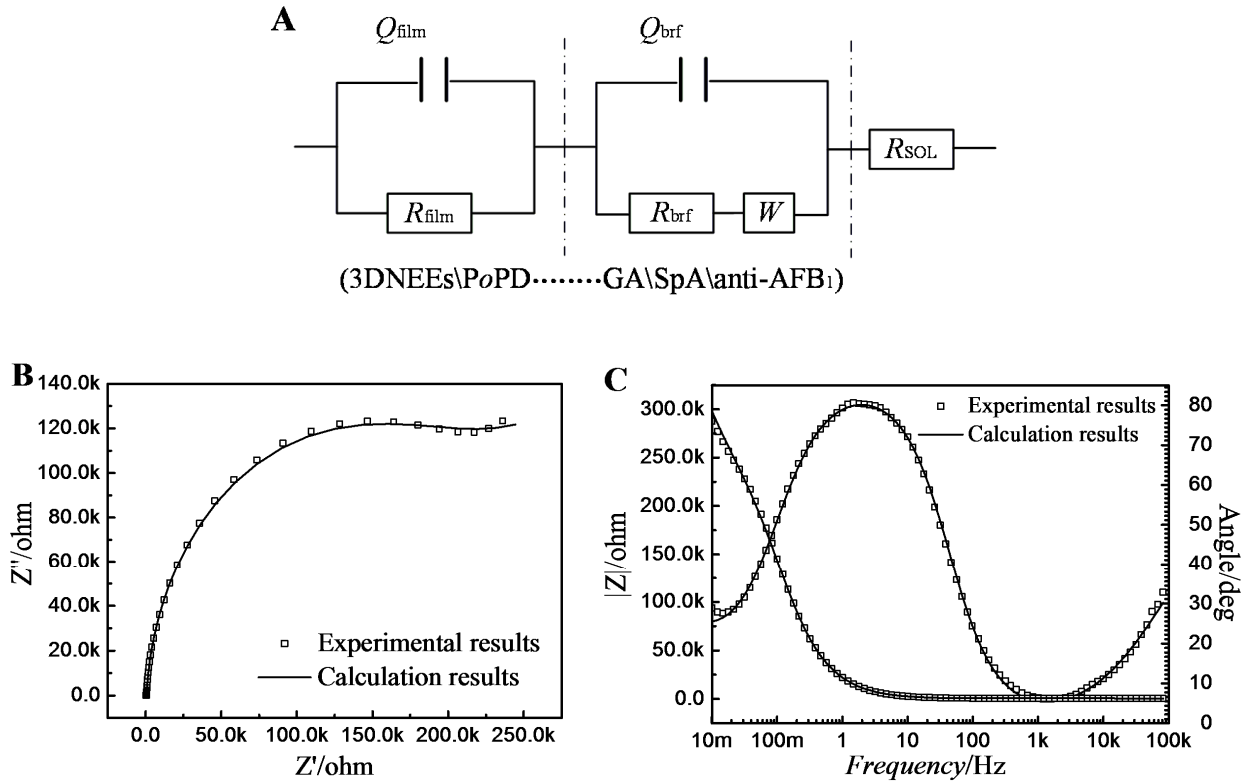

Fig. 7. Simulation circuit for the immunosensor in PBS (A); Comparison of the immunosensor response with the simulation circuit for Nyquist plots and Bode plots (B, C).

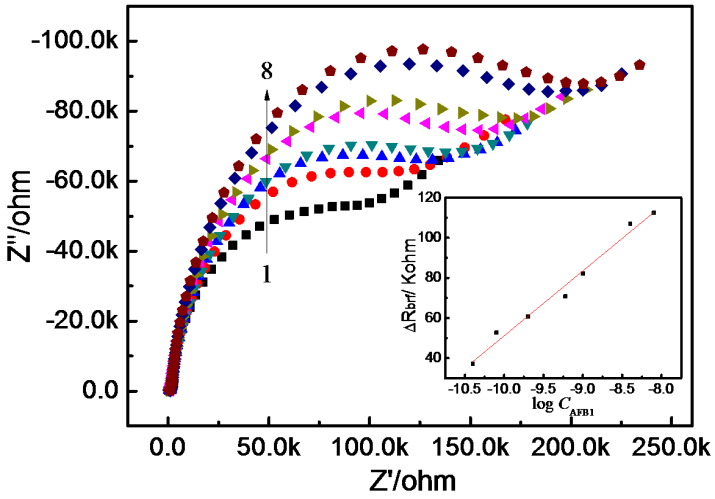

Fig. 8. Nyquist plots of the immunosensor in 0.2 mol/L PBS (pH 7.00) after immunity with the AFB1 diluents，concentrations ranging from 1 to 8 (0, 0.04, 0.08, 0.2, 0.6, 1.0, 4.0 and 8.0) ng/mL. Polarization potential: -150 mV vs. OCP, frequency range from 10 mHz to 100 KHz. The insert shows the calibration curve of ΔR_{brf} vs. logarithm concentration of AFB1 based on the Nyquist plots.

Fig 8 displays the Nyquist plots of the immunosensor response after immunity reaction in AFB_1 solution of different concentrations. By fitting the electrochemical impedance spectra to the equivalent circuit in Fig. 7 (A), the simulated values of all elements in equivalent circuit were summarized in table 2. Due to the good conductivity of support electrolyte, the R_{SOL} were relatively small. The R_{film} were around 1.1 kΩ and changed only a little with different AFB_1 concentrations, indicating that P*o*PD film prepared was stable and less affected by the specific immunity. The values of the constant phase element Q_{film} (~n_{film} 0.6) were small and fluctuated slightly, mainly owing to the capacitance produced by the conductive P*o*PD film.

The constant phase element Q_{brf} (~n_{brf} 0.8) in second loop is likely to be a physical capacity. A decrease in the Q_{brf} value with the increase of AFB_1 concentrations was found, which might be due to the variation of charged state of the biorecognition membrane caused by the formation of the bioaffinity complexes between anti-AFB_1 and AFB_1. The R_{brf} values continuously increased with AFB_1 concentrations, which may be ascribed to the formation of the complexes on the recognition membrane, passivating the electrode and blockage of the charge transfer of H^+ at the electrode/electrolyte interface. Further analysis showed that ΔR_{brf}, the difference of R_{brf} values before and after immunity exhibited a linear relationship to the logcarithm AFB_1 concentration in the range of 0.04 to 8.0 ng/mL (correlation coefficient, r=0.9812). The detection limit was estimated to be 0.019 ng/mL (*S*/*N*=3), which was about two orders of magnitude lower than 2 ppb (European Union limitation of AFB_1). The detection limit is lower than reported in literatures[13, 38] and the sensor has a larger detection range than other reported works.[39]

Table 2 Parameters resulting from the fitting of the Nyquist plots for biosensing process

c_{AFB1}/(ng/mL)	R_{SOL}/μΩ	Q_{film}/μF	n_{film}	R_{film}/kΩ	Q_{bif}/μF	n_{bif}	R_{bif}/kΩ	ΔR_{bif}/kΩ	W/μΩ
0	0.8107	0.9691	0.5824	1.084	14.13	0.8816	108.0	0	66.14
0.04	0.1036	0.3147	0.6459	1.074	13.08	0.8713	145.2	37.2	71.88
0.08	0.1321	0.3588	0.6373	1.108	12.32	0.8647	160.7	52.7	83.61
0.2	0.1236	0.2286	0.6679	1.195	11.83	0.8610	168.7	60.7	80.87
0.6	0.1327	0.1024	0.6656	1.165	10.94	0.8705	178.7	70.7	73.64
1.0	0.1074	0.3275	0.6457	1.113	8.92	0.8694	190.2	82.2	63.72
4.0	0.0967	0.4348	0.6231	1.190	8.68	0.8735	214.9	107.0	67.36
8.0	0.0963	0.3061	0.6504	1.154	8.07	0.8833	218.2	112.4	60.56

R_{SOL}: solution resistance, Q_{film}: film capacitance, R_{film}: film resistance, R_{brf}: charge transfer resistance of biorecognition film, Q_{brf}: capacitance of biorecognition film, W: Warburg resistance

Compared with our previous reported work[26] based on P*o*PD modified macro gold electrode, the present work performs in a wider range and has a lower detection limit. Our results on AFB_1/BSA/anti-AFB_1/GA/P*o*PD/3DNEEs without SpA showed that the ΔR_{brf} values exhibits a linear relationship to concentrations ranging from 3.0 to 100 ng/mL (correlation coefficient, r=0.9977). The detection limit was 1.5 ng/mL (*S*/*N*=3). The better performance of AFB_1/BSA/anti-AFB_1/SpA/GA/P*o*PD/3DNEEs could be ascribed to the function of P*o*PD/3DNEEs and SPA. The three dimensional structure and the rough surface of the 3DNEEs provide larger active area for immobilize more anti-AFB_1. SPA molecule combine the Fc fragment of anti-AFB_1 and make the antigen binding fragment (Fab fragment) extend outward orderly, and easier for combining AFB_1 antigen.[40, 41] However, the stability and service life of the immunosensor based on P*o*PD/3DNEEs were not satisfied, and not as good as that of the immunosensor based on macro gold electrode.

To evaluate the performance of the immunosensor, the determined unit of AFB_1-spiked corn samples were analyzed and the results are shown in table 3, which indicates that the developed impedimetric immunosensor is suitable for AFB_1 detection.

Table 3 The detected results of AFB_1 in spiked corn samples and recoveries

[AFB_1] added (ng/mL)	[AFB_1] found (ng/ml)	Recovery%
0.06	0.0535	89.2
0.60	0.541	90.2
6.00	6.35	105.8

4. Conclusions

An ultrasensitive label-free and time saving impedimetric immunosensor for AFB_1 based on P*o*PD/3DNEEs was designed and fabricated, and the interface model of molecular recognition was constructed. The high sensitivity, low detection limit and wide detection range for the detection of AFB_1 could be ascribed to the special structure and large active surface area of 3DNEEs, functionalizing features of the P*o*PD and the directional function of SpA.

The work in this paper provides a clue for designing an electrochemical immunosensor for AFB_1 detection, mycotoxins analysis and other electrochemical biosensors. However there will be a lot of work to do for its practical application, such as improving its preservation properties, service life and stability.

In addition, we think that designing and optimizing the 3DNEEs' structure and dimension will be very meaningful for its wider application in immunosensor.

Acknowledgements

This research work was supported financially by the National Natural Science Foundation of China (No. 21273056).

Notes and references

1 M. A. Klich, *Molecular Plant Pathology*, 2007, 8, 713-722.
2 S. H. Henry, F. X. Bosch, T. C. Troxell and P. M. Bolger, Science, 1999, 286, 2453-2454.
3 J. H. Williams, T. D. Phillips, P. E. Jolly, J. K. Stiles, C. M. Jolly and D. Aggarwal, Am J Clin Nutr, 2004, 80, 1106-1122.
4 G. J. B. Gnonlonfin, K. Hell, Y. Adjovi, P. Fandohan, D. O. Koudande, G. A. Mensah, A. Sanni and L. Brimer, Crit Rev Food Sci, 2013, 53, 349-365.
5 J. Stroka and E. Anklam, Trac-Trend Anal Chem, 2002, 21, 90-95.
6 N. H. S. Ammida, L. Micheli, S. Piermarini, D. Moscone and G. Palleschi, Anal Lett, 2006, 39, 1559-1572.
7 N. H. S. Ammida, L. Micheli and G. Palleschi, Anal Chim Acta, 2004, 520, 159-164.
8 S. Piermarini, L. Micheli, N. H. S. Ammida, G. Palleschi and D. Moscone, Biosens Bioelectron, 2007, 22, 1434-1440.
9 L. Micheli, R. Grecco, M. Badea, D. Moscone and G. Palleschi, Biosens Bioelectron, 2005, 21, 588-596.
10 I. Ben Rejeb, F. Arduini, A. Arvinte, A. Amine, M. Gargouri, L. Micheli, C. Bala, D. Moscone and G. Palleschi, Biosens Bioelectron, 2009, 24, 1962-1968.
11 Q. C. Li, L. X. Cao, H. F. Hu, K. Wang and P. S. Yan, Progress In Chemistry, 2014, 657-664.
12 M. H. Banitaba, S. S. H. Davarani and A. Mehdinia, Anal Biochem, 2011, 411, 218-222.
13 J. H. O. Owino, A. Ignaszak, A. Al-Ahmed, P. G. L. Baker, H. Alemu, J. C. Ngila and E. I. Iwuoha, Anal Bioanal Chem, 2007, 388, 1069-1074.
14 A. D. Chowdhury, A. De, C. R. Chaudhuri, K. Bandyopadhyay and P. Sen, Sensor Actuat B-Chem, 2012, 171-172, 916-923.
15 J. V. Rushworth, A. Ahmed, H. H. Griffiths, N. M. Pollock, N. M. Hooper and P. A. Millner, Biosens Bioelectron, 2014, 56, 83-90.
16 H. Wan, Q. Sun, H. Li, F. Sun, N. Hu and P. Wang, *Sensors and Actuators B: Chemical*, 2015, 209, 336-342.
17 M. Ongaro and P. Ugo, Anal Bioanal Chem, 2013, 405, 3715-3729.
18 F. Bottari, P. Oliveri and P. Ugo, Biosensors and Bioelectronics, 2014, 52, 403-410.
19 J. Moon, Y. Hui Kim and Y. Cho, Biosensors and Bioelectronics, 2014, 57, 157-161.
20 M. Arredondo, M. Stoytcheva, R. Zlatev and V. Gochev, Mini-Reviews in Medicinal Chemstry, 2012, 12, 1301-1313.
21 M. De Leo, A. Kuhn and P. Ugo, Electroanal, 2007, 19, 227-236.
22 K. Krishnamoorthy and C. G. Zoski, Anal Chem, 2005, 77, 5068-5071.
23 L. X. Cao, P. S. Yan, K. N. Sun and D. W. Kirk, Electrochim Acta, 2008, 53, 8144-8148.
24 L. X. Cao, P. S. Yan, K. N. Sun and D. W. Kirk, Electroanal, 2009, 21, 1183-1188.
25 P. Ugo, L. M. Moretto, M. Silvestrini and F. C. Pereira, Int J Environ An Ch, 2010, 90, 747-759.
26 N. N. Wu, L. X. Cao, P. S. Yan and M. H. Wang, Advanced Materials Research, 2011, 322, 385-389.
27 M. H. Wang, L. X. Cao, P. S. Yan and N. N. Wu, International Journal of Electrochemical Science, 2012, 7, 7927-7934.
28 J. Baniukevic, J. Kirlyte, A. Ramanavicius and A. Ramanaviciene, *Sensors and Actuators B: Chemical*, 2013, 189, 217-223.
29 N. Naveas, J. Hernandez-Montelongo, R. Pulido, V. Torres-Costa, R. Villanueva-Guerrero, J. P. García Ruiz and M. Manso-Silván, Colloids snd Surfaces B: Biointerfaces, 2014, 115, 310-316.
30 D. P. Meininger, M. Rance, M. A. Starovasnik, W. J. Fairbrother and N. J. Skelton, Biochemistry-Us, 2000, 39, 26-36.
31 V. P. Menon and C. R. Martin, Anal Chem, 1995, 67, 1920-1928.
32 D. H. JANG, Y. S. YOO and S. M. OH, B Kor Chem Soc, 1995, 16, 392-397.
33 L. L. Wu, J. Luo and Z. H. Lin, J Electroanal Chem, 1996, 417, 53-58.
34 A. C. Eliot and J. F. Kirsch, Annu Rev Biochem, 2004, 73, 383-415.
35 M. Graille, E. A. Stura, A. L. Corper, B. J. Sutton, M. J. Taussig, J. B. Charbonnier and G. J. Silverman, P NATL ACAD SCI USA, 2000, 97, 5399-5404.
36 S. Bilal, A. Ali Shah and R. Holze, Electrochim Acta, 2011, 56, 3353-3358.
37 E. Gongadze, K. Bohinc, U. van Rienen, V. Kralj-Iglič and A. Iglič, in Advances in Planar Lipid Bilayers and Liposomes, Academic Press, Editon edn., 2010, vol. Volume 11, pp. 101-126.
38 L. T. Zhou, R. Y. Li, Z. J. Li, Q. F. Xia, Y. J. Fang and J. K. Liu, Sensor Actuat B-Chem, 2012, 174, 359-365.
39 H. Ghosh and C. RoyChaudhuri, 2012 Sixth Internayional Conference on Sensing Technology (ICST), 2012, 688-693.
40 J. Zhou, L. Du, L. Zou, Y. Zou, N. Hu and P. Wang, *Sensors and Actuators B: Chemical*, 2014, 197, 220-227.
41 J. Z. Sun, C. Bian, L. Qu and S. H. Xia, Chinese Journal of Analytical Chemistry, 2009, 484-488.